Int. J. Electrochem. Sci., 10 **(2015)** 8656 - 8667

International Journal of
ELECTROCHEMICAL
SCIENCE
www.electrochemsci.org

Effect of Oilfield Produced Water on Corrosion of Pipeline

Xin Wang[1], *Jin Xu*[2,*], *Cheng Sun*[2], *MaoCheng Yan*[2]

[1] Shenyang Broadcasting and Televisioin University, Institute of Science and Technology, Biochemistry Department, Shenyang China, 110003
[2] Environmental corrosion center, Institute of Metals Research,Chinese Academy of Sciences, Shenyang China, 110016.
[*]E-mail: xujin@imr.ac.cn

Received: 23 June 2015 / *Accepted:* 28 July 2015 / *Published:* 26 August 2015

Metals, such as 16Mn steel, can be attacked by produced waters, causing serious corrosive problems in systems such as equipments and pipelines in processes of recycling and reuse of produced-waters. In this paper, effects of the produced-water taken obtained from Xinjiang oilfield on the corrosion and scaling with temperature and time are investigated by electrochemical methods and micro-analyses. The results show that the corrosion rate of 16 Mn steel arrives at a peak at 70℃in the produced-water, and corrosion type is pitting. Information of formation of scales can be acquired by EIS analysis. The scales are formed on the surface of the corrosion products.

Keywords: Corrosion; Scaling; 16 Mn steel; high temperature; produced-water

1. INTRODUCTION

Oilfield produced-water is formed during the processes of petroleum exploration and utilization, and is considered to be wastewaters. In order to decrease the consumption of clean water and protect the environment, it is necessary to find an effective way to reuse these waste waters, especially in water-deficient regions [1-2]. The benefits of recycling and reusing produced-water include not only a saving of vast quantities of fresh water, but also an absolute recovery of the thermal energy. However, compared with fresh water, produced-water contains abundant corrosive substrates [3-4], which will result in a significant threat to safe operation and also leads to huge economic losses. Thus, studies of effects of the produced-water on corrosion of the pipelines and the equipments in the petroleum industry have become more and more important. There are many studies of effects of the produced-water [5-9]. Migahed et al. [10] studied effects of inhibitors on corrosion behavior of X65 steel in CO_2 saturated oil well produced water. The result showed that the selected inhibitor is mixed

type, and could inhibit both cathodic and anodic reaxtions. Silva et al. [11] investigated corrosion and inhibition of carbon steel in the simulating produced water generated in oil and gas extraction by weight loss, electrochemical methods and surface analysis. They indicated that the simulated produced water W_1 had a lower corrosion rate than W_2, and iron dissolution was accompanied with an adsorbed intermediary species, $FeOH_{ads}$. Zhang et al. [12] studied corrosion behavior of X65 carbon steel in simulated oilfield produced water, and found that acetic acid and CO_2 had a synergistic effect on the steel. Zhang et al. [13] investigated the inhibiting effect of sophorolipids on the corrosion of X65 steel in the simulated oilfield produced water. sophorolipids were an anodic-type inhibitors. The above studies mainly concentrated on appraisal of inhibitor and corrosion of the steel in the simulated oilfield produced water. However, there has been little research on the effects of "real" produced-water on corrosion of the pipeline and the equipment during the process of recycling and reuse of the produced-water.

In this study, the effects of produced-water taken from Xinjiang oilfield on corrosion and scaling of the 16 Mn steel are investigated by using electrochemical methods, X-ray power diffractometer (XRD), scanning electron microscopy (SEM), and EDAX.

2. EXPERIMENTAL

2.1. Produced water

Table 1. Analysis results of produced-water in Xinjiang oilfield

Parameter	Ion concentration (mg/L)								Total alkalinity (mmol/L)	Total hardness (mmol/L)	Total dissolved solid (mmol/L)
Concentration	Mg^{2+}	Ca^{2+}	$Na^{+}+K^{+}$	Fe^{2+}	Cl^{-}	SO_4^{2-}	HCO_3^{-}	SiO_2			
	119.1	357.9	6056	0.08	9225	165	366	51	6.6	27.66	16175.1

The produced-water was collected from the sewage treatment station, Xinjiang oilfield. The properties of produced-water from high pour-point crude oil are listed in Table 1, and pH of the water is 8.1.

2.2. Coupon

Standard coupon I (16 Mn steel sheets, size: 10 × 10 × 3 mm) for the electrochemical measurement had a composition of (wt.%): 0.15 C, 1.36Mn, 0.24 Ni, 0.41 Si, 0.027 S, 0.022 P, 0.26 Cr, 0.21 Cu. And the balance was Fe, and hen embedded in epoxy resin to prepare test sample with an exposed surface area of 2.25 cm^2 for electrochemical measurements. The coupons were abraded with a series of grit papers (200, 400, 600, and 800) followed by cleaning in acetone and alcohol and dried.

2.3. Simulating experimental facility

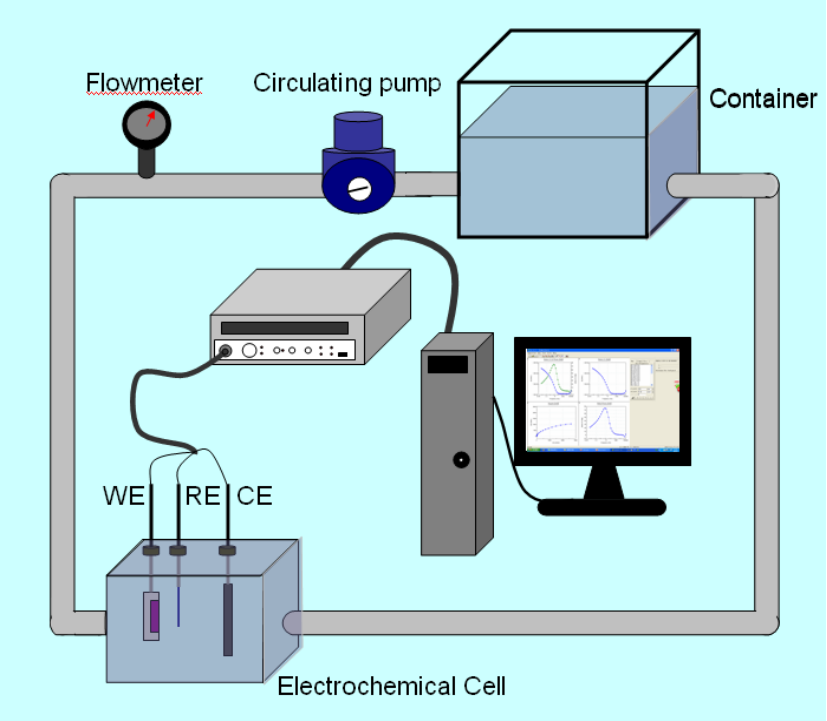

Figure 1. Schematic diagram of the simulated experimental facility

A simulating experimental system was designed, as showed in Fig. 1, which included a container, a circulating pump, a flowmeter, and a electrochemical cell. The produced water was filled in the container equipped with a heating system, which could control the temperature of the water. During the experimental process, deionized water was added in the beaker every 4 h to compensate the loss of water via evaporation and maintain the concentrations of different ions and reagents in the water samples. The pump was used to control flowing rates of the water, and the rate was at the constant speed of 0.5 m/s. A three-electrode cell, with a graphite electrode used as the counter electrode, and a platinum electrode as the reference electrode, was set at the system to conduct electrochemical measures in the electrochemical cell.

2.4. Electrochemical measurement

The electrochemical analysis was used to investigate the electrochemical properties of the corroded surface. All experiments were performed in a three-electrode electrochemical cell, with a graphite electrode used as the counter electrode, and a platinum electrode as the reference electrode. The test was operated using the PARSTAT 2273 electrochemical measurement system manufactured by the EG&G. The potential range of the Linear polarization was from -10 mV to +10 mV at the open circuit potential with the scanning rate of 0.166 mV/s, The frequency range of the EIS was from 0.001 Hz to 100 kHz and the amplitude of the sinusoidal voltage signal was 10 mV. The EIS data obtained were modeled and simulated using the Zsimpwin software supplied by the PARSTAT2273.

2.5. SEM and EDXA

A scanning electron microscope (XL30-FEG) with the beam voltage at 25 kV was used to visualize the morphology of surface, and an energy dispersive X-ray spectroscopy (EDXA) system was for elemental analysis.

3. RESULTS AND DISCUSSION

3.1. Variation with temperature

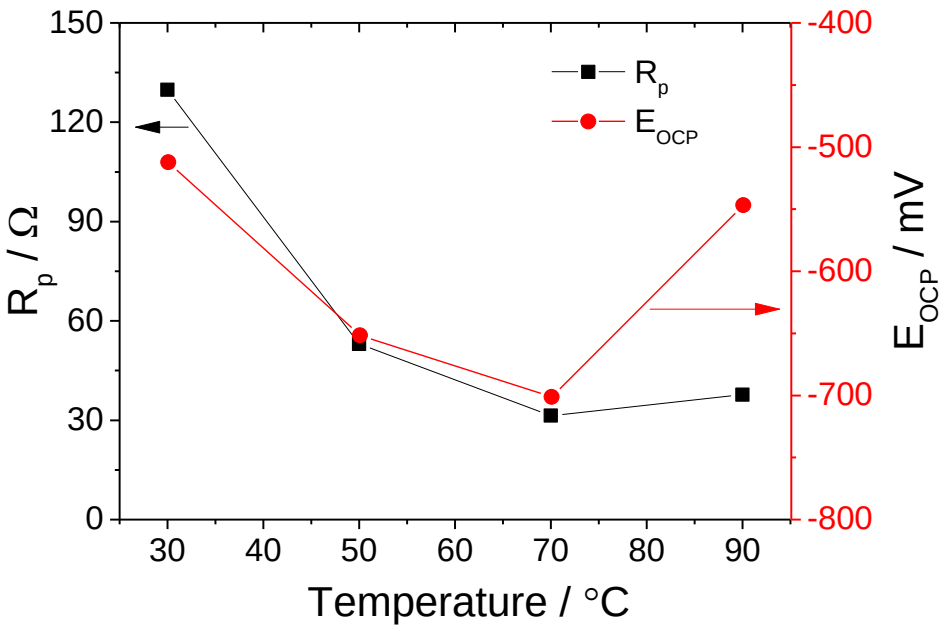

Figure 2. Variations of R_p and E_{OCP} with temperature after 24 h

Figure 2 shows the variations of R_p measured by linear polarization and E_{OCP} with temperature after immersing for 24 h. It can be seen that the potential of the steel decreases with temperature, reaching the minimum value at a temperature of 70 ℃, and then increase. The varying tendency of the R_p of the steel is similar to that of the E_{OCP}, the minimum value also appear at 70 ℃. As mentioned by Zhang et al. [12], the corrosion rate increased with the increase of temperature in the simulated produced water. It is consistent with the variation of the corrosion rate below 70 ℃in our studies. The corrosion rate still increases when the temperature is beyond 70 ℃ because there are not any substances that can form the scales in the simulated solutions. Based on the knowledge [14], the process of the scales formation usually occurs at high temperatures of 80-90℃. As a result, when the temperature is higher than 70 ℃, the scale begins to be formed on the surface of the steel, and this scale is protective, which leads to the decreasing of the corrosion rate. The above result indicates that the corrosion rate of the steel reaches a peak in the produced water at 70 ℃.

Table 2. Fitting results of EIS with temperature

Temperature ℃	R_s Ω• cm^2	R_f Ω• cm^2	Y_f mS•se c^n/cm^2	n_f	R_t Ω• cm^2	Y_{dl} mS•se c^n/cm^2	n_t	R_L Ω• cm^2	L H•cm^2
30	52.56	42.83	4010	0.8299	112.8	0. 448	0.676	26.06	49.02
50	36.25	23.42	8460	0.8303	42.02	0. 683	0.8778	22.1	40.35
70	22.68	9.092	13.4	0.7376	20.42	1.4	0.8682	7.587	14.69
90	21.94	7.817	0.162	0.8393	25.68	0. 379	0.9153	18.43	26.88

The EIS plots of the steel and the equivalent circuit are given in figure3 at different temperature after 24 h, and the fitting results are listed in Table 2. In the electrical analog circuits, R_s represents an electrolyte resistance, R_f and CPE_f represent a resistance and a capacitance of the film of the corrosion products, R_t and CPE_{dl} represent a charge transfer resistance and a double layer capacitance, and R_L and L represent a inductive resistance and a inductance, respectively. As shown in Fig. 3, three time constants are observed, viz., there are two capacitive loops in the high and middle frequency, and an inductive loop in the low frequency.

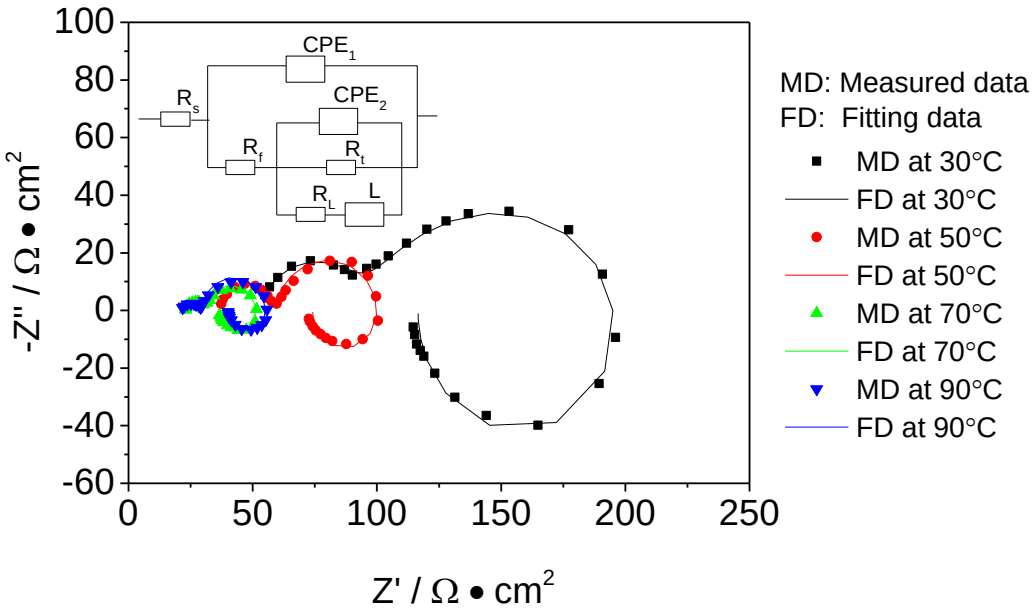

Figure 3. Variations of EIS with temperature after 24 h

R_t is considered as a standard for assessing the corrosion rate of the metal. From Fig. 3 and table 2, R_t decreases with increasing of the temperature, reaching the minimum value at the temperature of 70 ℃, and then increase. This result shows that the corrosion rate of the steel is the highest at 70 ℃. It is accordance with the result of the linear polarization.

Ion activities in the produced water increase with the increasing of the temperature, which leads to the increasing of the corrosion rate of the steel. However, with the further increasing of the temperature, the effect of the forming of the scales on the corrosion gradually increases. The scales can prevent the corrosive ions from diffusing onto the interface of the steel, which further inhibit the corrosion of the steel. The above reasons lead to the appearance of the maximum rate at 70 ℃.

Inductive loops can be observed at the low-frequency regions from the EIS plot, Fig. 3. The inductive loop often has a relationship with the intermediate product adsorbed on the surface of the steel [15-16], which is formed during the process of corrosion reaction. It is accordance with the result by Zhang et al. [12].

3.2. Variation with time

Long-period experiment was conducted in order to investigate the long-period effect of the produced water on corrosion of the steel at high temperature. The test temperature is selected to be 70 ℃ according to the above experiment. Fig. 4 shows the variations of R_p and E_{OCP} with time at the temperature of 70 ℃. The potential decreases with time, and then remains stable after immersing for 5 days, fluctuating at the potential of about 600 mV. R_p of the steel increases with time, and then remains stable after 18 days, which indicates that the corrosion rate of the steel is stable after 18 days. The increasing of R_p and positive shift of the potential is due to the formation of protective films including the corrosion products and scales. With reaching a balance between forming rate and dissolution rate of the films, the value of R_p and the potential are stable [17].

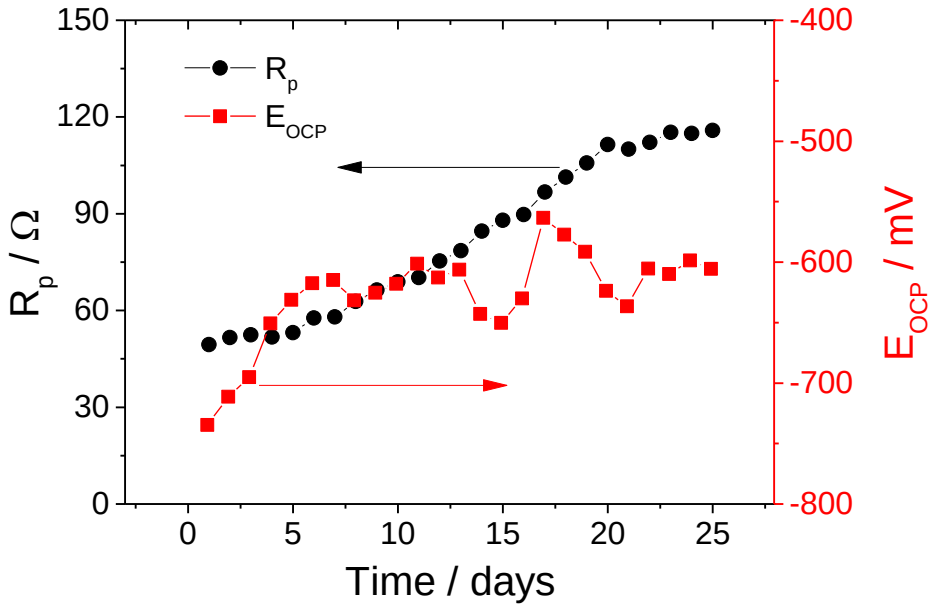

Figure 4. Variations of R_p and E_{OCP} with time at the temperature of 70 ℃

Figure 5 shows the EIS plots of the steel and the equivalent circuit with time at the temperature of 70℃, and the fitting results are listed in Table 3.

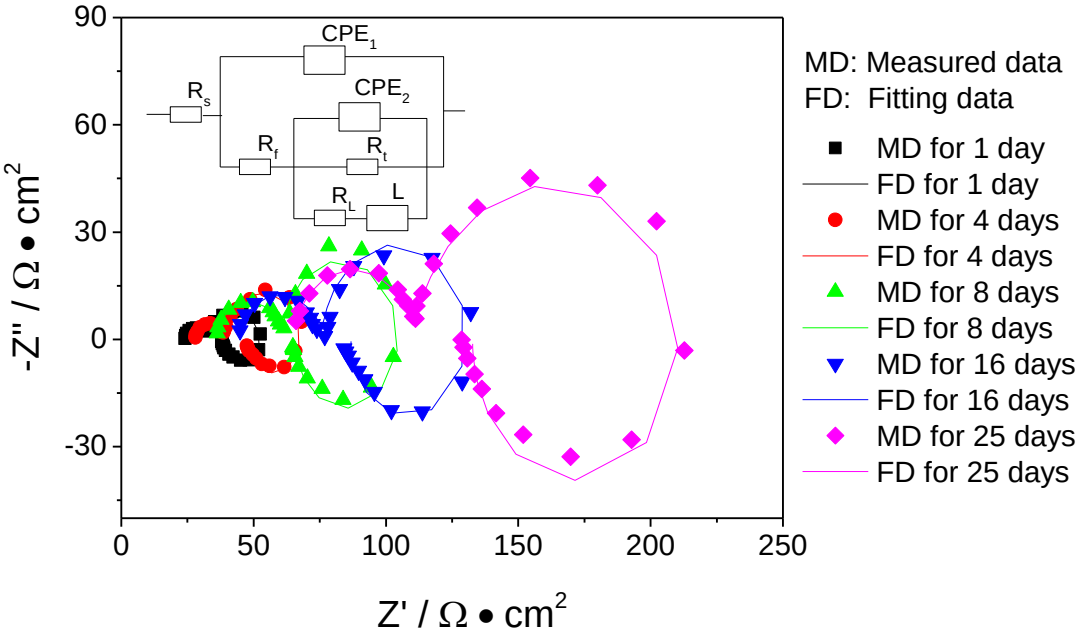

Figure 5. Variations of EIS with time at the temperature of 70 ℃

Table 3. Fitting results of EIS with time

Time day	R_s Ω• cm^2	R_f Ω• cm^2	Y_f mS•se c^n/cm^2	n_f	R_t Ω• cm^2	Y_{dl} mS•se c^n/cm^2	n_t	R_L Ω• cm^2	L H•cm^2
1	23.82	8.406	367	0.8107	21.63	1.926	0.8082	9.286	13.87
4	27.69	11.34	222	0.8365	30.01	1.266	0.9146	13.79	18.49
8	35.33	26.1	6500	0.865	43.51	0. 483	0.9995	4.758	14.1
16	43.27	33.32	8380	0.8165	55.67	0. 736	0.9675	12.46	25.12
25	64.48	46	1830	0.9003	108.1	0. 565	0.8636	28.03	61.61

As shown in Fig. 3 and table 2, R_t increases with time, reaching 108.1 Ω•cm^2 after immersing for 25 days. This is due to the forming of the corrosion products and the scales. This composite film might prevent transport of corrosive ions and inhibit the anodic and cathodic reactions, which results in the decreasing of the rate.

From the relationship between capacitance and time (Fig. 6), the capacitance of the corrosion product layer decreases with time, which indicate that the corrosion product layer becomes more and more compact, and its protection against corrosion of the steel gradually become strong. The capacitance of the double electric layer also decreases with time, which leads to increasing of the

resistance that the corrosive ions cross the double electric layer. These two results both result in the decreasing of the corrosion rate of the steel.

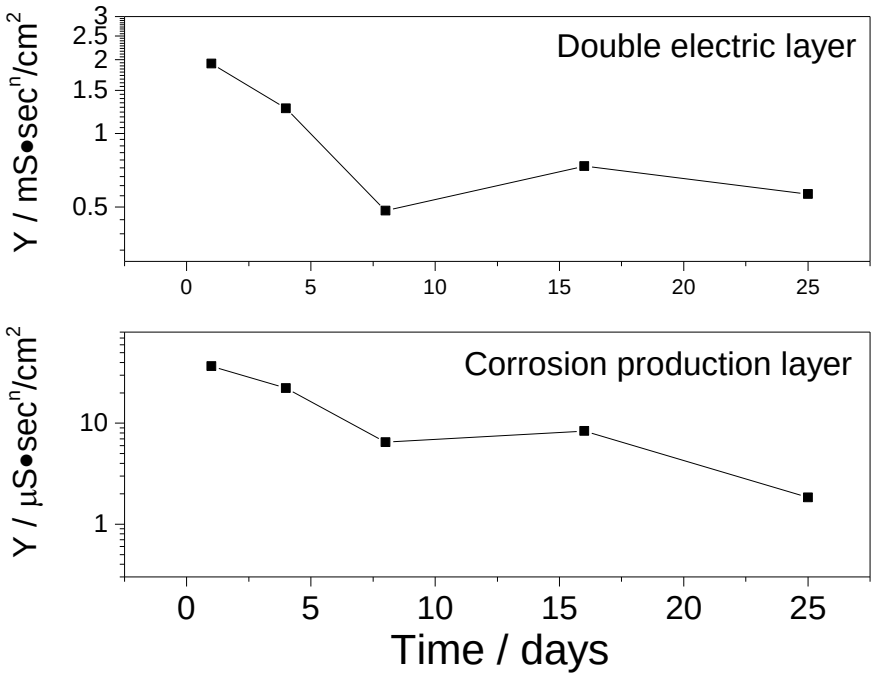

Figure 6. Variations of capacitance with time at the temperature of 70 ℃

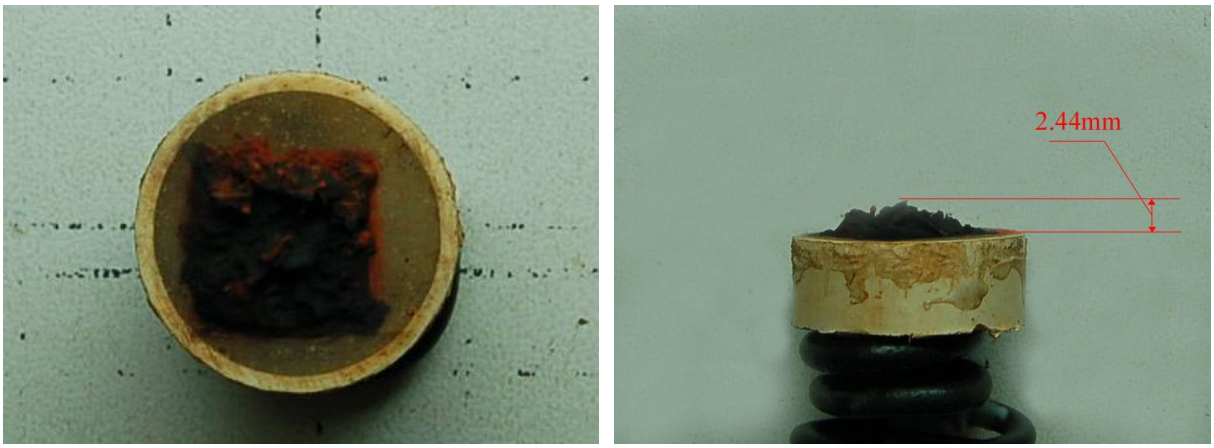

Figure 7. Appearance of corrosion of the steel after immersing for 25 days

It can also been seen from table 3 that R_s increases with time, and the value after 25 days reaches nearly 3 times as large as that after 1 day. This variation trend is reversed to the results of normal corrosion experiment [17-18]. As we all know, the ionic concentrations of solutions increase with corrosion reaction proceeding, which leads to increasing of electrical conductivity of solutions and decreasing of resistance of solutions. The solution resistance usually decreases with time in the immersing experiment due to the increasing of ionic concentration caused by corrosion of the steel.

This might be due to the formation of the scales on the surface of the steel, and this layer of the scales was considered as a pure resistance. It can be seen from the appearance of the steel (Fig. 7) that a layer of the scales is formed on the surface of the steel, and the maximum of the scale thickness is 2.44 mm. According to this result, the forming of the scales can be judged by the variations of the solution resistance in the EIS plots.

3.3 Micrographic analysis

Figure 8 shows XRD result of the loose products of the outer. It contains $CaCO_3$, SiO_2, Fe_3O_4, and FeO(OH), which indicate that the products are composed of amounts of the scales and a little the corrosion products. After removing the loose products, the inner product is analyzed by XRD, as shown in Fig. 9. Only Fe_3O_4 and Fe are observed on the surface of the steel, not any phase of the scales. The above results indicate that the steel reacts with the corrosive ions at the beginning, the corrosion products are formed on the surface of the steel, and then the scales are deposited on the surface of the loose products.

The produced water is mainly composed of $CaCl_2$ type in Xinjiang oilfield, and contains large amounts of Ca^{2+} and HCO_3^- ions. Therefore, $CaCO_3$ scale layer will be formed when a large number of OH^- meet these scale ions. Furthermore, due to the existence of the dissolved oxygen, Cl^- ion and other inorganic salts are the main influence factors for the corrosion and scaling in the produced water. Liu et al. investigated water injection pipe in Tuba oil and analyzed the corrosion products and scales. They found that $CaCO_3$ and FeO(OH) are observed in the products in the pipe [20].This is similar to our conclusion.

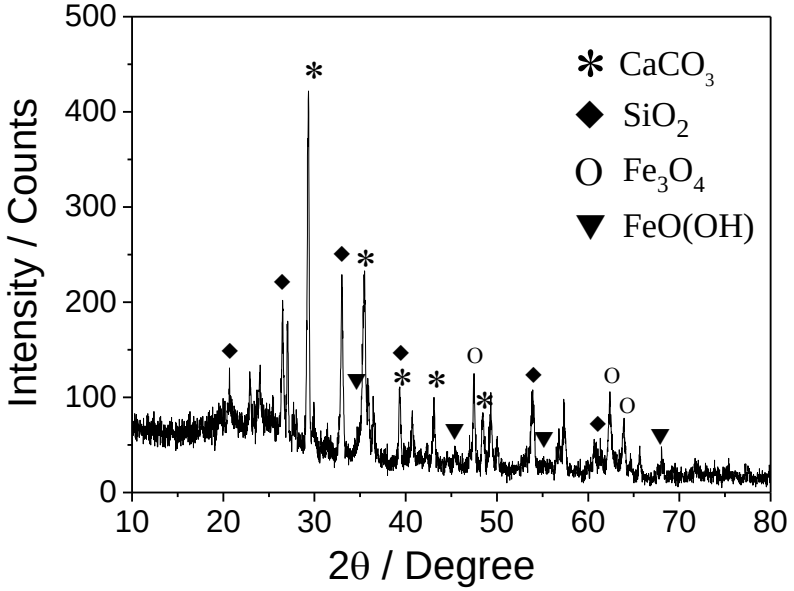

Figure 8. XRD result of the products on the surface of the steel

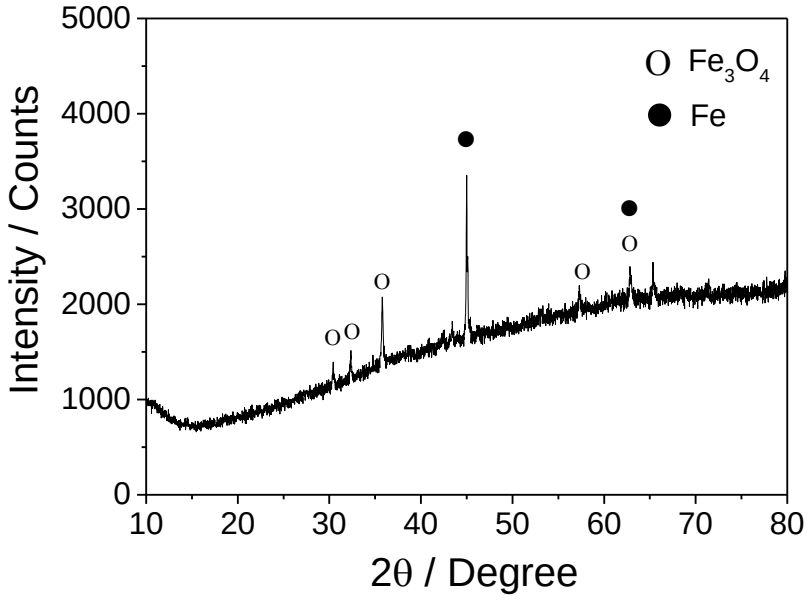

Figure 9. XRD result of the corrosion product on the surface of the steel

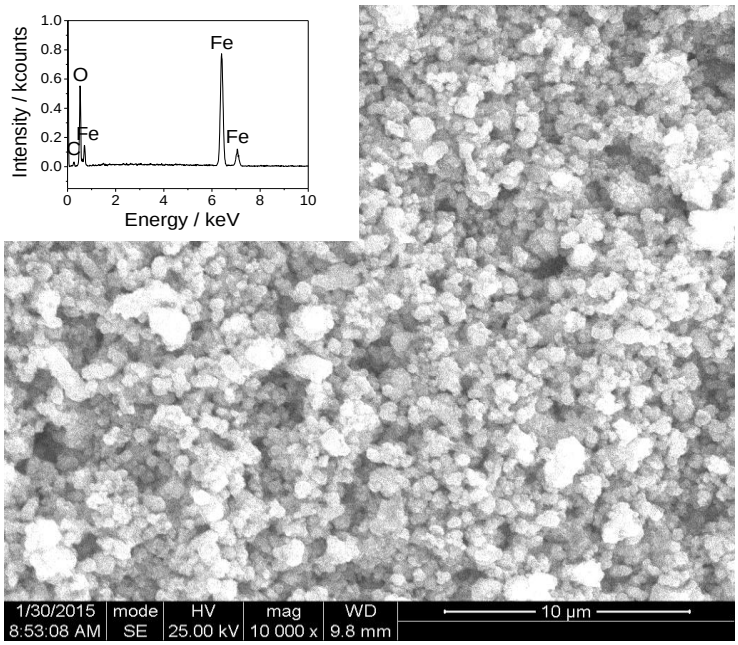

Figure 10. SEM and EDXA of the corrosion products after removing the scales

SEM and EDXA of the corrosion products after removing the loose scales are given in Fig. 10. There are a large amount of flocculent corrosion products on the surface of the steel, but they are relative dense. Liu et al. also found that a layer of dense film is formed on the coupon in laboratory [20]. These corrosion products are iron oxide from the EDXA results.

The steel has been severely corroded after the corrosion products are removed from the surface, as shown in Fig. 11. Amounts of pitting holes are observed on the surface, which indicate that the corrosion type of the steel in the produced water is local corrosion, mainly pitting.

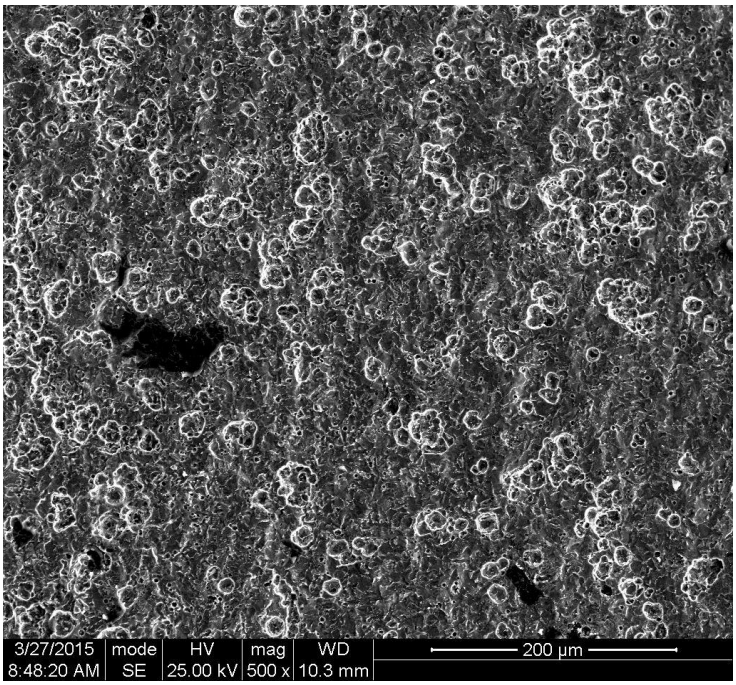

Figure 11. SEM of the steel after removing the corrosion products

4. CONCLUSION

(1) The corrosion rate of the steel reaches the maximum value at the temperature of 70 ℃ in the produced water.

(2) The variation of the scales can be analyzed by the solution resistance of EIS, and the scales become thicker with the increasing of the solution resistance.

(3) The scales do not deposit on the surface of the corrosion products until forming of the corrosion products.

ACKNOWLEDGEMENTS
We are grateful for financial support of the National Natural Science Foundation of China (Grant Nos. 51471176)

References

1. R. Martínez-Palou, M. Mosqueira, B. Zapata-Rendón, E. Mar-Juárez, C. Bernal-Huicochea, J. Clavel-López and J. Aburto, *J. Petrol. Sci. Eng.*, 75 (2011) 274.
2. M.A. Ameer, A.M. Fekry and A. Othman, *Int. J. Electrochem. Sci.*, 9 (2014) 1964.
3. E.S. Mona, R. Mahmoud and A.M. Thanaa, *Desalination*, 249 (2009) 748.

4. X.Y. Liu, J.G. Li, Q.Y. Zhu, J.L. Feng, Y.L. Li and J.X. Sun, *J. Petrol. Sci. Eng.*, 66 (2009) 161.
5. Gang Li, Shuhai Guo, Jiangwei Zhang and Yu Liu, *Desalination*. 351 (2014) 213.
6. M.M. Jordan, C.J. Graff and K.N. Cooper, *SPE Prod. Facil.*, 16 (2001) 267.
7. M.B. Tomson, G. Fu, M.A. Watson and A.T. Kan, *SPE Prod. Facil*., 18 (2003) 192.
8. M. Amiri and J. Moghadasi, *Petrol. Sci. Techno.*, 30 (2012) 453.
9. J.W. Zhang, G. Li and Y. Liu, *Adv. Mater. Res.*, 734-737 (2013) 2214.
10. M. A. Migahed, M. M. Attya, M. Abd El-raouf, E. A. Khamis1, T. A. Ali and A. M. Al-Sabagh, *Int. J. Electrochem. Sci.*, 10 (2015) 1343.
11. A. B. da Silva, J. A. C. P. Gomes, E. D. Elia, M. J. C. Rezende, A. C. Pinto and B. N. M. Silva, *Int. J. Electrochem. Sci.*, 8 (2013) 9317.
12. Y. L. Zhang, M. Du, J. Zhang and J. Q. Du, *Mater. Corros.*, 66 (2015) 366.
13. J. Zhang, J. Wang, F.M. Zhu and M. Du, *Ind. Eng. Chem. Res.*, 54 (2015) 5197.
14. G. Li, S.H. Guo, J.W. Zhang and Y. Liu, Desalination, 351 (2014) 213.
15. Z. F. Yin,W. Z. Zhao,W. Y. Lai, C. X. Yin and S. D. Zhu, J.Mater. Eng. Perform., 19 (2010) 693.
16. M. Kedam, O. R. Mattos and H. Takenouti, J. Electrochem. Soc., 128 (1981) 257.
17. D. Starosvetsky, O. Khaselev, J. Starosvetsky, R. Armon and J. Yahalom, Corros. Sci., 42 (2000) 345.
18. J. Xu, C. Sun, M.C. Yan, F.H. Wang, *Int. J. Electrochem. Sci.*, 7 (2012) 11281.
19. J. Xu, C. Sun, M.C. Yan, F.H. Wang, *Int. J. Electrochem. Sci.*, 7 (2012) 11297.
20. Y.C. Liu, Y.L. Zhang and J.M. Yuan, Eng. Fail. Anal., 45 (2014) 225.